Materials Science & Engineering A 639 (2015) 136–144

Contents lists available at ScienceDirect

Materials Science & Engineering A

journal homepage: www.elsevier.com/locate/msea

Three different alumina–zirconia composites: Sintering, microstructure and mechanical properties

Heidy L. Calambás Pulgarin, María P. Albano *

Centro de Tecnología de Recursos Minerales y Cerámica (CETMIC), C.C. 49 (B1897ZCA) M. B. Gonnet, Provincia de Buenos Aires, Argentina

ARTICLE INFO

Article history:
Received 3 December 2014
Received in revised form
9 April 2015
Accepted 3 May 2015
Available online 12 May 2015

Keywords:
Al_2O_3–ZrO_2
Sintering behavior
Microstructure
Mechanical properties

ABSTRACT

Two commercial 3 mol% yttria–partially stabilized zirconia powders, with 0.3 wt% Al_2O_3 (Y–PSZA) and without Al_2O_3 (Y–PSZ), and a Zr (IV) precursor were used to produce alumina (Al_2O_3)–zirconia (ZrO_2) slip cast composites. The influence of both the zirconia content and the reduction of zirconia particle size on the sintering behavior, microstructure development and mechanical properties were investigated. The increase in the zirconia content from 10.5 to 22 vol% increased the hardness; whereas, above 22 vol% ZrO_2 the hardness decreased. A significant increase in the fracture toughness with increasing the ZrO_2 content over 22 vol% was obtained by the stress-induced phase transformation. The flaw size limited the strength below 22 vol%; whereas, above 22 vol% ZrO_2 the strength was controlled by the stress-activated phase transformation. For 10.5 vol% ZrO_2, the smaller ZrO_2 grains produced by using the Zr (IV) precursor were more effective in preventing the Al_2O_3 grain growth resulting in higher hardness. However, the tetragonal–monoclinic (t–m) transformation of some unstabilized ZrO_2 grains during cooling reduced Young's modulus and fracture toughness.

1. Introduction

The mechanical behavior of zirconia-toughened-alumina ceramics is currently of great interest, mainly as a result of their high strength and enhanced fracture toughness [1]. The stress-induced martensitic transformation of tetragonal zirconia can markedly increase the fracture toughness of alumina–zirconia ceramics. In order to retain the tetragonal phase to room temperature, it is found that both the addition of Y_2O_3 stabilizer and the reduction of ZrO_2 grain size are required [2]. In this work, two commercial 3 mol% yttria–partially stabilized zirconia powders, with 0.3 wt% Al_2O_3 (Y–PSZA) and without Al_2O_3 (Y–PSZ), were used to produce Al_2O_3–ZrO_2 slip cast composites. The Al_2O_3 content play an important role for the densification of Y–PSZ ceramics. Matsui [3] explained the enhanced effect of Al_2O_3 on the densification of Y–PSZ with a change of the principal diffusion mechanism from grain-boundary to bulk volume diffusion. We have also studied [4] the enhanced sintering effect of Y–PSZ with 0.3 wt% Al_2O_3 compared to Y–PSZ in the sintering of 50 vol% Al_2O_3–50 vol% ZrO_2 composites.

Al_2O_3 and ZrO_2 ceramics can be produced by conventional powder processing techniques which involve mixing, pressing and subsequent sintering. Slip casting is a suitable consolidation process to obtain compacts with high sintered densities and microstructural homogeneity allowing the manufacture of components with complex shapes [1]. According to Requena et al. [5] the slip casting technique is a powerful method to obtain Al_2O_3 and Al_2O_3/ZrO_2 multilayer composites with nearly theoretical density ($>98\%$).

In a recent paper we reduced the ZrO_2 particle size by using a Zr (IV) precursor route [6]; smaller particles with respect to the classical powder mixing route, homogeneously distributed on the Al_2O_3 particle surfaces were obtained. Szutkowska [7] studied the fracture resistance behavior of sintered alumina–10 wt% zirconia (≈ 7 vol% ZrO_2) produced either with unstabilized ZrO_2 or 3 mol% yttria–partially stabilized zirconia powders; he measured the fracture toughness of these composites and pure alumina by different methods. His results showed that the alumina–10 wt% zirconia composites with unstabilized ZrO_2 had the highest fracture toughness value independently on the used method. In this paper, a series of Al_2O_3–ZrO_2 formulations were prepared either by using the two commercial 3 mol% Y–PSZ powders or a Zr (IV) precursor. The influence of both the zirconia content and the reduction of zirconia particle size on the sintering behavior and microstructure

* Corresponding author. Fax: +54 221 471 0075.
E-mail address: palbano@cetmic.unlp.edu.ar (M.P. Albano).

http://dx.doi.org/10.1016/j.msea.2015.05.010
0921-5093/

development were studied. In addition, the effect of these microstructures on the mechanical properties were discussed.

2. Experimental procedure

2.1. Raw materials and powder processing

Alumina (A16 SG, Alcoa Chemicals, USA, $d_{50}=0.40$ μm), 3 mol% yttria–partially stabilized zirconia with 0.3 wt% Al_2O_3 (Saint-Gobain ZirPro, CY3Z-MA, Chine, $d_{50}=0.23$ μm) and without Al_2O_3 (Saint-Gobain ZirPro, CY3Z-NS, Chine, $d_{50}=0.64$ μm) powders were used in this study. For the colloidal method, zirconium (IV)-propoxide solution (70 wt% in 1-propanol) (Sigma-Aldrich, Ireland) was added dropwise to a stable alumina (A16) suspension in absolute ethanol; this method was described in a previous paper [6]. The compositions used to prepare Al_2O_3–ZrO_2 composites are summarized in Table 1.

A commercial ammonium polyacrylate solution (NH_4PA) (Duramax D 3500, Rohm and Haas, Philadelphia PA) was used as deflocculant. 48 vol% aqueous Al_2O_3–ZrO_2 suspensions with the different compositions (Table 1) and the optimum NH_4PA concentration were prepared by suspending particles in deionized water via 40 min of ultrasound; the pH was manually adjusted to be maintained at 9 with ammonia (25%). Slips were cast in plaster molds into rectangular bars ($12\times10\times9$ mm^3); the consolidated bars were dried slowly in air for 24 h at room temperature and 24 h at 100 °C. The green samples were sintered in air at 1100–1600 °C for 2 h (heating rate 5 °C/min).

2.2. Characterization techniques

The specific surface area (S_g) and the particle size distribution of the powders were measured using a Micromeritics Accusorb and a Sedigraph (Micromeritics), respectively.

The density of the green compacts was determined by the Archimedes method using mercury displacement. The bulk density of the sintered samples was determined by water immersion (Standard Method ASTM C20). An impulse excitation frequency tester (GrindoSonic, MK5 Model) was used to determine the Young's modulus. The measured resonant frequency, along with the length, thickness, wide and weight of the bars were used in the following equation to calculate Young's modulus:

$$E = 0.9465\left(\frac{mf_f^2}{w}\right)*\left(\frac{L^3}{e^3}\right)*T_1 \quad (1)$$

where m is the specimen mass, w is the wide, L is the length, f_f is the frequency (Hz), e is the specimen thickness and T_1 is the shape factor (depedent on Poisson's ratio). Five measurements were tested for each sample and the results are presented as mean values. Theoretical values of Young's modulus were determined for comparison using a rule of mixtures in the form $E=E_1\nu_1+E_2\nu_2$; where E_1 and ν_1 are the modulus values and volume fraction of Al_2O_3, respectively, and E_2 and ν_2 are the respective values of ZrO_2.

The mechanical properties evaluated for the samples sintered at 1600 °C were hardness, fracture toughness (K_{1c}) and flexural strength. The sintered samples were polished with a series of diamond pastes down to 1/4 μm and annealed at 1100 °C for 30 min to remove surface strains introduced during machining. The Vickers hardness (Hv) was carried out using a diamond indenter (Buehler hardness tester) and calculated as follows:

$$\mathrm{Hv} = 1.854\frac{F}{d^2} \quad (2)$$

where F is the indentation load and d is the arithmetic mean of two diagonals (d_1 and d_2). 10 Hv measurements were used to obtain an average value.

The fracture toughness (K_{1c}) was calculated on the basis of the indentation method:

$$K_{1C} = 0.016\left(\frac{E}{\mathrm{Hv}}\right)^{1/2}\frac{P}{C^{3/2}} \quad (3)$$

where E is Young's modulus, Hv is the vickers hardness, P is the indentation load and C is the crack length, which was measured using the ocular on the hardness tester. The flexural strength of the sintered samples was measured using a three-point bending test (INSTRON, 4483). About 10 measurements of fracture toughness and flexural strength were tested for each sample and the results are presented as mean values.

The alumina and zirconia grain sizes were measured using SEM micrographs (JEOL, JSM-6360) of polished and thermally etched surfaces. The grain size values were the average of about a hundred measurements.

The percentages of monoclinic and tetragonal ZrO_2 in the composites were determined by XRD analysis (Philips 3020 equipment, with Cu-Kα radiation in Ni filter at 40 kV to 20 mA) using the Rietveld method [8].

Table 1
Compositions used for the preparation of Al_2O_3–ZrO_2 composites and green density of slip cast compacts.

Sample[a]	Al_2O_3 (vol%)	Y–PSZA (vol%)	Y–PSZ (vol%)	ZN (vol%)	Green density (% DT)[b]
10.5Y–PSZA	89.5	10.5	–	–	63.2
10.5Y–PSZ	89.5	–	10.5	–	64.3
10.5ZN	89.5	–	–	10.5	57.0
22Y–PSZA	78	22	–	–	62.5
22Y–PSZ	78	–	22	–	64.8
22ZN	78	–	–	22	54.0
50Y–PSZA	50	50	–	–	60.0
50Y–PSZ	50	–	50	–	65.3

[a] The numbers 10.5, 22 and 50 in the sample codes indicate the volume percent of zirconia in the composite.
[b] Theoretical density.

3. Results and discussion

3.1. Powder characterization

Fig. 1 a shows the particle size distribution curves of the Al_2O_3, Y–PSZ and Y–PSZA powders. In Fig. 1b the particle size distribution curves of the 10.5 and 22ZN powders after milling were compared with that of Al_2O_3. Alumina showed a unimodal distribution with particle diameters >0.1 and <0.75 μm, the more frequent particle diameters were in the range of 0.15–0.3 μm. A slightly narrow particle size distribution was found for Y–PSZA; thus a greater volume of finer particles (diameters between 0.10 and 0.20 μm) and a lesser volume of particles with diameters in the range of 0.20–0.55 μm were observed, the more frequent particle diameter was 0.15 μm. A bimodal distribution curve was found for Y–PSZ, the more frequent particle diameters (0.37 and 0.65 μm) were greater than those of Al_2O_3 and Y–PSZA powders.

A slightly wider particle size distribution was found for the ZN powders with respect to that of Al_2O_3 (Fig. 1b); a lesser volume of finer particles (<0.35 μm) and a greater volume of particles with diameters in the range of 0.35–0.9 μm were found. The more frequent particle diameters of 10.5ZN were in the same range as those of Al_2O_3; whereas, for the 22ZN powder the more frequent particle diameters became greater (0.40–0.60 μm). Although the Zr

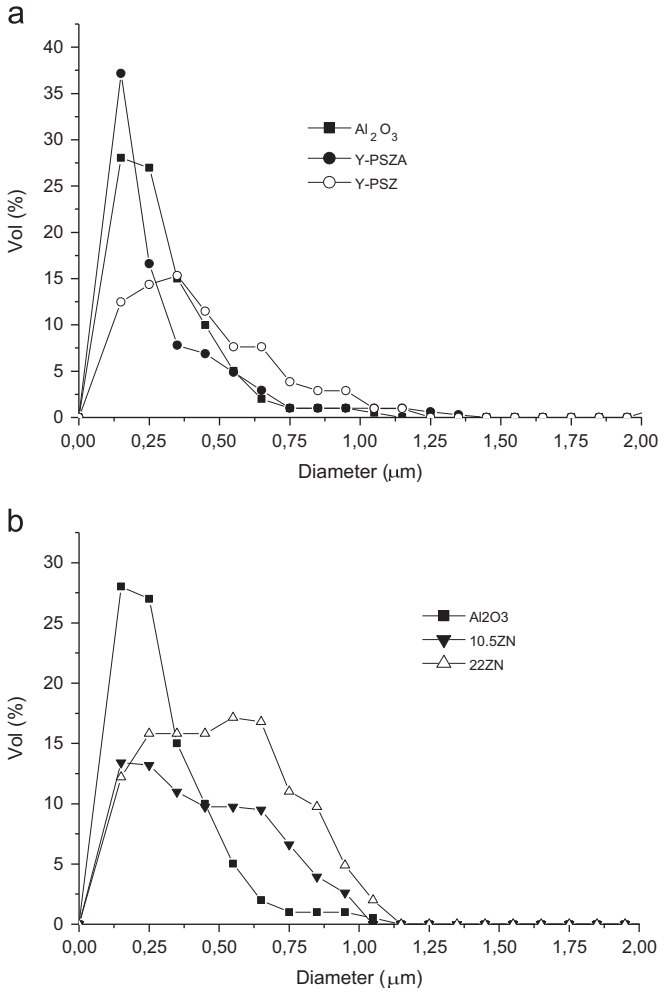

Fig. 1. Particle size distribution curves of different as-received powders: (a) Al_2O_3, Y–PSZ and Y–PSZA; and (b) Al_2O_3, 10.5 and 22ZN powders after milling.

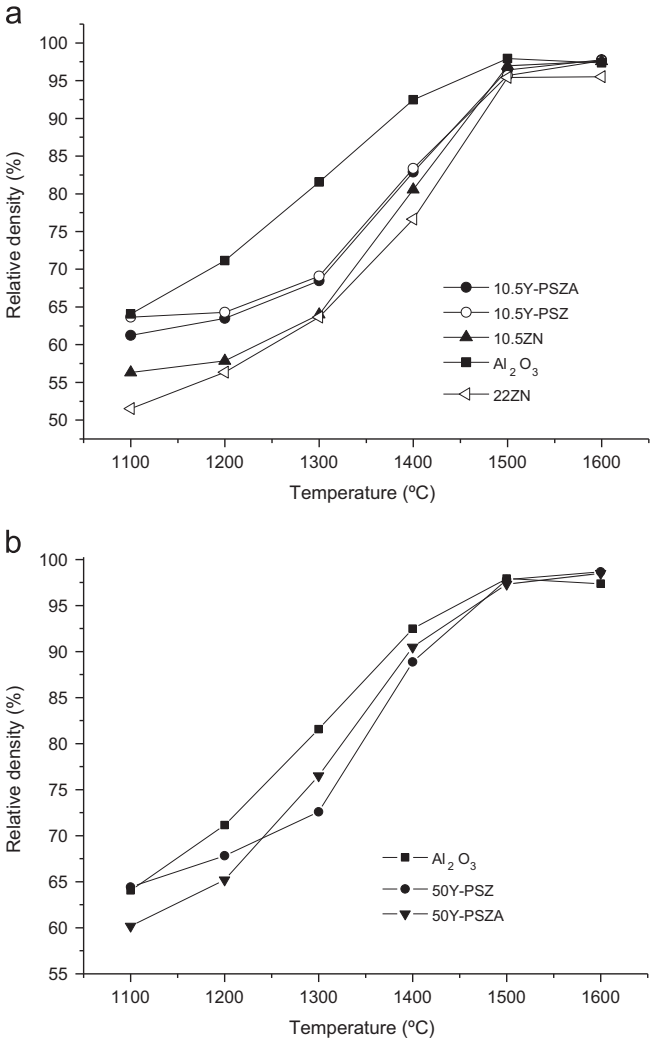

Fig. 2. Relative sintered density versus sintering temperature curves of Al_2O_3 and the composites with different ZrO_2 contents: (a) 10.5 vol% ZrO_2 and 22ZN, (b) 50 vol% ZrO_2.

(IV) precursor route avoided the formation of ZrO_2 aggregates on the Al_2O_3 particles [6], it let to aggregates of some Al_2O_3 particles with very fine ZrO_2 uniformly distributed. The diameters of the Al_2O_3 aggregates increased with increasing the ZrO_2 content.

The specific surface area (S_g) of Al_2O_3, Y–PSZ, Y–PSZA, 10.5ZN and 22ZN powders was 8.74, 7.84, 12.25, 9.7 and 13 m^2/g, respectively. The finer particles of Y–PSZA was responsible to its higher specific surface area with respect to that of Al_2O_3 and Y–PSZ. The higher S_g of the ZN powders with respect to that of Al_2O_3 was attributed to the fine-sized ZrO_2 on the Al_2O_3 particles [6].

3.2. Densification and grain growth

Table 1 shows the green density values of the different Al_2O_3–ZrO_2 composites. For Al_2O_3-Y–PSZ compacts, green density values between 64.3% (10.5Y–PSZ) and 65.3% (50Y–PSZ) of theoretical density were found; while for Al_2O_3-Y–PSZA compacts, the green density had values between 63.2% (10.5Y–PSZA) and 60.0% (50Y–PSZA) of theoretical density. In a recent paper [6], we compared the green density of the different Al_2O_3–ZrO_2 composites and related them to the degree of slip dispersion. The substitution of Y–PSZ by Y–PSZA in the Al_2O_3–ZrO_2 mixtures increased the slip viscosity with NH_4PA resulting in a less dense packing of cast samples [6]. The cast samples obtained from the Al_2O_3–ZN slips exhibited the lowest green density values, 57.0% and 54.0% of the theoretical density for 10.5 and 22ZN, respectively (Table 1). This behavior was attributed to the presence of some aggregated particles in the slips which increased the resistant to flow [6].

Fig. 2a shows the change in the relative sintered density with sintering temperature of Al_2O_3, 22ZN and the different composites with 10.5 vol% ZrO_2; Fig. 2b shows the corresponding curves of Al_2O_3 and the composites with 50 vol% ZrO_2. The respective Delta sintered density with respect to Delta temperature ($\Delta\rho/\Delta T$) are shown in Fig. 3a and b. The relationship between the relative density and the sintering temperature for 22Y–PSZA and 22Y–PSZ showed nearly the same behavior as 10.5Y–PSZA and 10.5Y–PSZ, respectively. The densification behavior of Al_2O_3 and the different composites could be related with the Al_2O_3 mean grain diameter measured at the different temperatures (Table 2). The Al_2O_3 grain diameter in pure Al_2O_3 remained nearly constant in the temperature range 1100–1250 °C, then a slightly increase in the grain diameter with increasing sintering temperature up to 1400 °C was found; thereafter an important increase in the Al_2O_3 grain diameter up to 1600 °C was observed (Table 2). When the Al_2O_3 average grain diameter increased over about 1 μm at 1400 °C a markedly decrease in the sintering rate of Al_2O_3 was found (Table 2 and Figs. 2 and 3). At temperatures above 1400 °C the porosity changed from being open and interconnected to closed and isolated and simultaneously grain growth occurred.

The densification rate of 10.5Y–PSZA and 10.5Y–PSZ showed a maximum at 1330 °C (Fig. 3a); at temperatures > 1300 °C the Al_2O_3 grains began to grow, a slightly increase in the Al_2O_3 grain diameter between 1300 and 1500 °C was found followed by an important increase from 1500 to 1600 °C (Table 2). In the temperature range 1330–1450 °C the atomic transport process resulted in densification with a lesser contribution of coarsening; at $T > 1450$ °C the larger contribution of coarsening reduced the sintering rate (Fig. 3a and Table 2).

For 10.5ZN the densification rate increased with an increase in the sintering temperature up to reaching a plateau in the range 1350–1450 °C, afterwards a rapidly decrease from 1450 °C to 1600 °C was found (Fig. 3a). The Al_2O_3 grain size measurements showed negligible grain growth up to 1400 °C, thereafter a gradual increase in the Al_2O_3 grain diameter up to 1600 °C was observed (Table 2). However, the Al_2O_3 grain diameter obtained at 1600 °C was lower than that found for 10.5Y–PSZA and 10.5Y–PSZ. The presence of fine ZrO_2 grains by using the Zr (IV) precursor not only delayed the onset of Al_2O_3 grain growth until the temperature reached 1400 °C, but also reduced the Al_2O_3 grain growth up to 1600 °C (Table 2). Thus, the ZrO_2 efficiency in preventing Al_2O_3 grain growth was significantly increased by reducing the ZrO_2 grain size. This was attributed to the pinning effect which was associated to the locations of small ZrO_2 grains at the intergranular boundaries and often the triple junctions between Al_2O_3 grains, preventing the Al_2O_3 grain growth. The pinning effect was shown in Fig. 4a, the bright ZrO_2 grains indicated by arrows are at the triple points between the dark Al_2O_3 grains. These results were in good agreement with those of Requena et al. [5]; who measured an alumina average grain size of ≈5.5 μm and ≈3.5 μm in Al_2O_3 and Al_2O_3/ZrO_2 (4 vol% ZrO_2) slip cast layers sintered at 1625 °C, respectively.

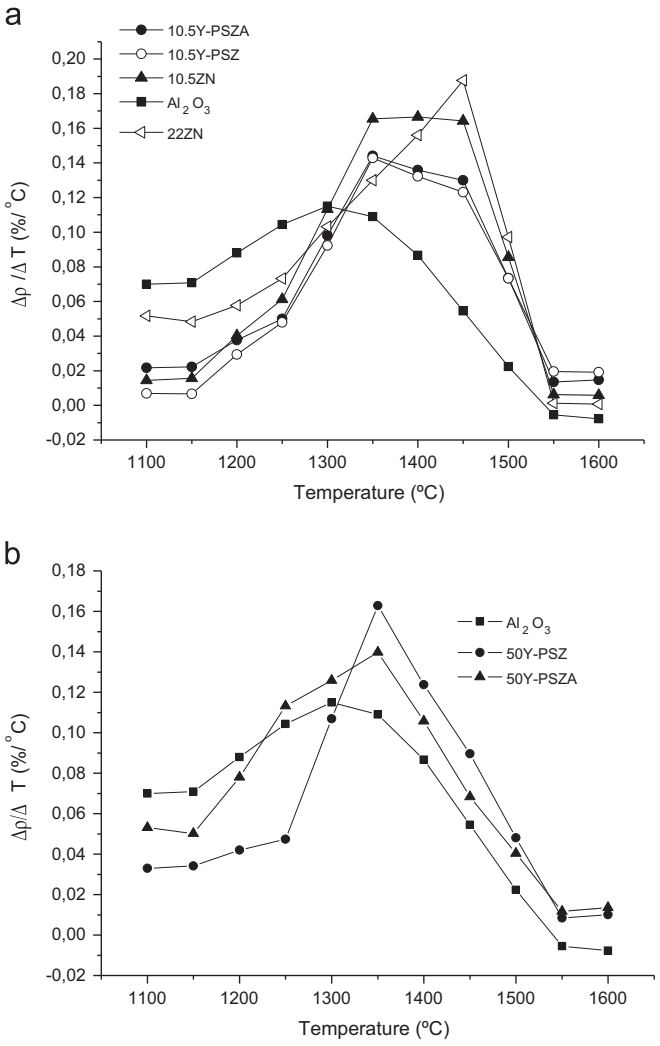

Fig. 3. $\Delta\rho/\Delta T$ (%/°C) versus sintering temperature for Al_2O_3 and the composites with different ZrO_2 contents: (a) 10.5 vol% ZrO_2 and 22ZN, (b) 50 vol% ZrO_2.

The temperature of maximum densification of 22ZN was shifted to 1450 °C (Fig. 3a); this composite exhibited a greater increase in the Al_2O_3 mean grain diameter with temperature at 1400–1600 °C than that observed for 22Y–PSZA and 22Y–PSZ (Table 2). The aggregated Al_2O_3 particles in the green state also produced aggregation of the fine ZrO_2 particles, increasing the ZrO_2 grain size during sintering. Therefore, the effect of the small ZrO_2 grains size in preventing Al_2O_3 grain growth could not be expected in this composite. Besides, a high sintered density at 1600 °C could not be achieved due to the low packing density of the green compacts (Fig. 2a). Therefore, this composite will not be considered in the subsequently study on mechanical properties.

The densification rates of 50Y–PSZA and 50Y–PSZ at the intermediate sintering temperature were both lower than that of Al_2O_3 (Figs. 2b and 3b); however, 50Y–PSZA began to sinter at lower temperatures with respect to 50Y–PSZ and higher relative densities at 1250–1400 °C could be achieved. The variation in Al_2O_3 grain diameter with sintering temperature of the two composites with 50 vol% ZrO_2 was similar in the investigated temperature range (1100–1600 °C) (Table 2). During the intermediate stage of sintering (1250–1400 °C), the 50Y–PSZA densified faster than the 50Y–PSZ one; however, at $T > 1450$ °C the densification rate of both composites became similar and remained almost identical until the final temperature was reached (Figs. 2b and 3b). These results indicated that the starting Y–PSZA powder characteristics strongly influence the intermediate sintering stage, during which the surface diffusion was prevailing. The enhanced sintering effect of 50Y–PSZA with respect to 50Y–PSZ at the intermediate sintering stage was studied in a previous paper [4]; we explained that the higher sintering rate of 50Y–PSZA could be attributed to the increase in the specific surface area of the powders together with the enhanced densification produced by the Al_2O_3 content. The densification rate of Al_2O_3 at the intermediate

Table 2
Al_2O_3 mean grain diameters (d_{50}) of the samples as a function of sintering temperature (d_{50} Al_2O_3 ± 0.05 μm).

Temperature (°C)	d_{50} Al_2O_3 Al_2O_3 (μm)	d_{50} Al_2O_3 10.5Y–PSZA (μm)	d_{50} Al_2O_3 10.5Y–PSZ (μm)	d_{50} Al_2O_3 10.5ZN (μm)	d_{50} Al_2O_3 22Y–PSZA (μm)	d_{50} Al_2O_3 22Y–PSZ (μm)	d_{50} Al_2O_3 22ZN (μm)	d_{50} Al_2O_3 50Y–PSZA (μm)	d_{50} Al_2O_3 50Y–PSZ (μm)
1100	0.40	0.30	0.31	0.30	0.32	0.31	0.31	0.30	0.30
1200	0.44	0.34	0.35	0.31	0.36	0.35	0.36	0.31	0.31
1250	0.48	0.38	0.39	0.31	0.40	0.40	0.41	0.32	0.32
1300	0.70	0.43	0.44	0.32	0.44	0.45	0.46	0.33	0.33
1400	1.03	0.88	0.83	0.32	0.51	0.60	0.69	0.34	0.35
1500	2.20	1.12	1.08	0.75	0.81	0.92	0.96	0.52	0.54
1600	4.21	1.84	2.08	1.19	1.33	1.50	1.58	0.75	0.80

sintering stage was higher than that of all the Al_2O_3–ZrO_2 composites (Fig. 2a and b). This was due to the lower activation energy of Al_2O_3 with respect to that of Al_2O_3–ZrO_2 [9].

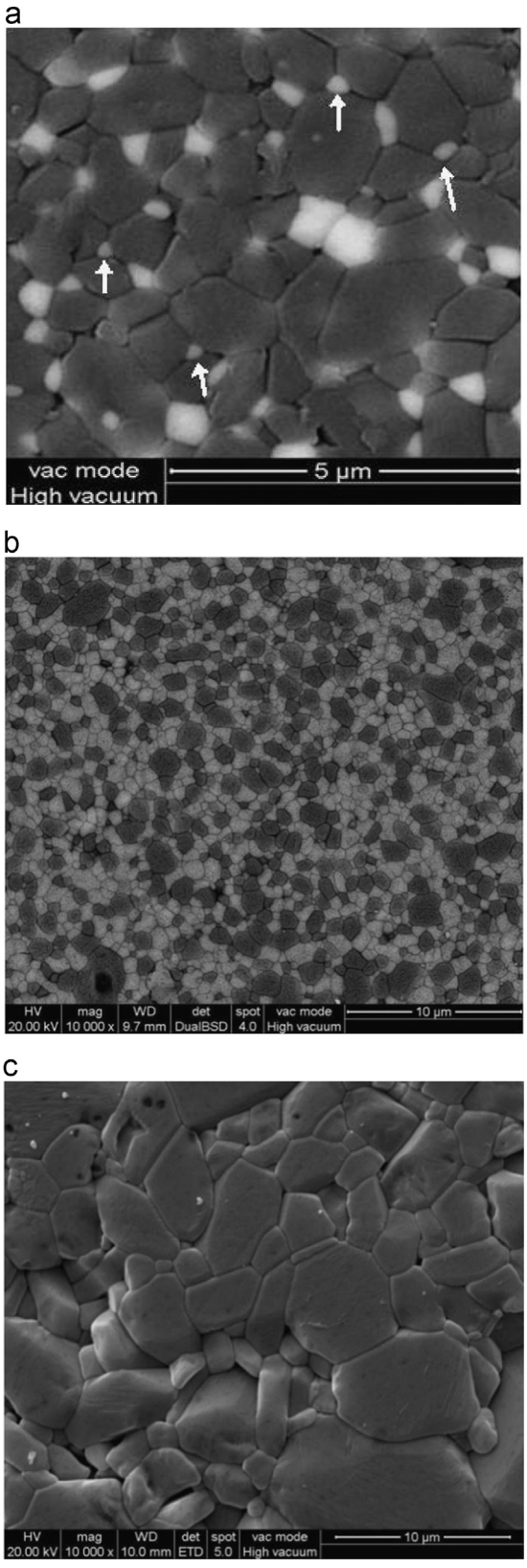

Fig. 4. SEM micrographs of different samples sintered at 1600 °C: (a) 10.5ZN showing the pinning effect, the bright ZrO_2 grains indicated by arrows are at the triple points between the dark Al_2O_3 grains, (b) 50Y–PSZ, and (c) Al_2O_3.

Table 3
ZrO_2 mean grain diameters (d_{50}) of the composites as a function of sintering temperature (d_{50} $ZrO_2 \pm 0.05$ μm).

Temperature (°C)	d_{50} ZrO_2 10.5Y–PSZA (μm)	d_{50} ZrO_2 10.5Y–PSZ (μm)	d_{50} ZrO_2 10.5ZN (μm)	d_{50} ZrO_2 22Y–PSZA (μm)	d_{50} ZrO_2 22Y–PSZ (μm)	d_{50} ZrO_2 50Y–PSZA (μm)	d_{50} ZrO_2 50Y–PSZ (μm)
1300	0.30	0.30	0.30	0.31	0.31	0.31	0.31
1400	0.30	0.30	0.30	0.31	0.31	0.31	0.31
1450	0.36	0.37	0.37	0.38	0.38	0.40	0.42
1500	0.42	0.43	0.43	0.44	0.46	0.51	0.60
1550	0.53	0.56	0.50	0.59	0.63	0.70	0.78
1600	0.64	0.71	0.56	0.72	0.79	0.82	0.95

The pinning effect became larger as the ZrO_2 concentration in the composites increased from 10.5 to 50 vol%; a greater number of ZrO_2 grains reduced the contacts between Al_2O_3 grains and consequently the Al_2O_3 grain boundary mobility resulting in a lesser Al_2O_3 grain growth (Table 2). For pure Al_2O_3 the rapid grain growth at 1400–1600 °C let to a grain diameter at 1600 °C that was about 5.3 times greater than the grain diameter obtained in the presence of 50 vol% ZrO_2 (Fig. 4b–c and Table 2); thus, 50 vol% ZrO_2 was the most effective concentration in inhibiting Al_2O_3 grain growth. Both the presence of small ZrO_2 grains homogeneously distributed within the matrix and the increase in the ZrO_2 content decreased the contacts between Al_2O_3 grains and effectively reduced the Al_2O_3 grain-boundary mobility.

For all the composites, the ZrO_2 mean grain diameter remained constant at 1300–1400 °C (Table 3). The fine ZrO_2 grains of the composite 10.5ZN began to grow at 1400 °C, thereafter a gradual increase in the ZrO_2 grain diameter up to 1600 °C was found. For 10.5Y–PSZ and 10.5Y–PSZA a lower increase in the grain diameter with increasing sintering temperature up to 1500 °C was observed, followed by rapid grain growth with further increasing in temperature up to 1600 °C; leading to a grain diameter at 1600 °C greater than that obtained for 10.5ZN (Table 3).

The increase in the ZrO_2 content from 10.5 to 22 vol% produced a slightly increase in the ZrO_2 grain diameter at 1500–1600 °C (Table 3). An increase in the ZrO_2 concentration over 22 vol% increased the contacts between ZrO_2 grains approaching each other and promoting their growth; thus the largest ZrO_2 grain diameter in the composites with 50 vol% ZrO_2 at 1500–1600 °C occurred by the coalescence of the ZrO_2 grains.

As the zirconia content increased the Al_2O_3 grain growth was lesser whereas the ZrO_2 grain growth became greater; thus, the ratio of Al_2O_3 to ZrO_2 grain sizes decreased with increasing amounts of ZrO_2. The ZrO_2 grain diameter distribution curves for 10.5 and 50 vol% ZrO_2 are shown in Fig. 5a and b, respectively. For 10.5 vol% ZrO_2 (Fig. 5a), a greater volume of grains with diameters in the range 0.6–1 μm were found for 10.5Y–PSZA and 10.5Y–PSZ with respect to 10.5ZN. The most frequent grain diameter of 10.5ZN was 0.4 μm, a low percentage of ZrO_2 grains had diameters between 0.75 and 1 μm. On the contrary, the most frequent grain diameter of 10.5Y–PSZA and 10.5Y–PSZ was shifted to a greater grain diameter of 0.62 and 0.68 μm, respectively. Thus, finer ZrO_2 grains could be obtained at 1600 °C by the Zr (IV) precursor route. The 50Y–PSZ curve was shifted to greater grain diameters with respect to that of 50Y–PSZA (Fig. 5b). The most frequent grain diameter was 0.7 and 0.9 μm for 50Y–PSZA and 50Y–PSZ, respectively. The smaller ZrO_2 grain diameter at 1600 °C for 50Y–PSZA with respect to 50Y–PSZ was attributed to the lesser grain growth of Y–PSZA relative to that of Y–PSZ at the final sintering stage (1500–1600 °C) (Table 3). Thus, for the composites with 50 vol% ZrO_2 the 0.3 wt% Al_2O_3 content in the starting Y–PSZ powder not only increased the sintering rate at

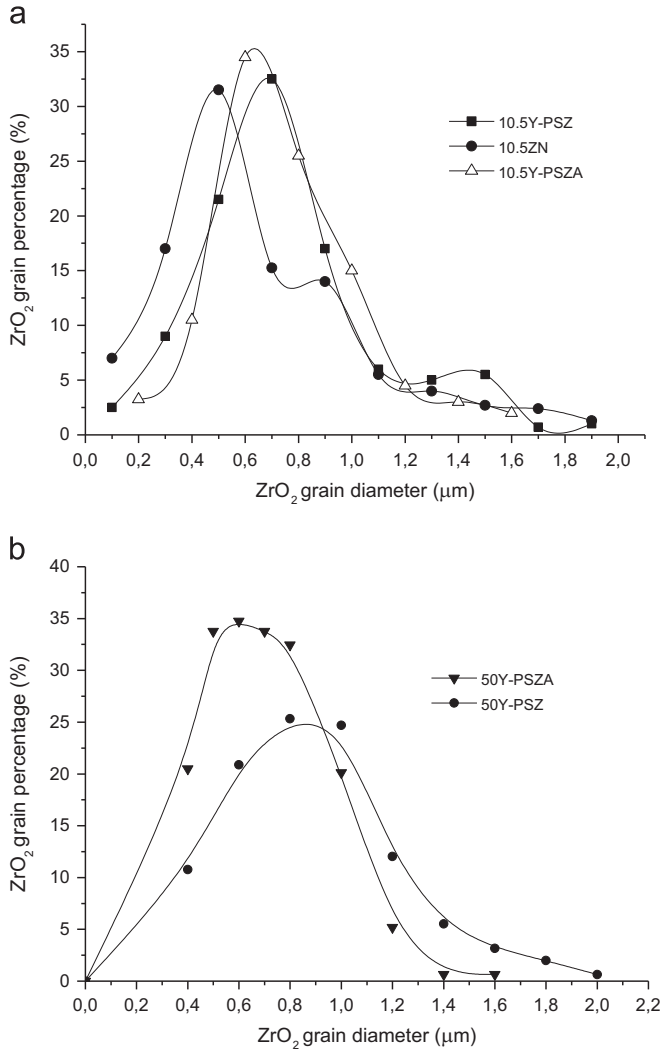

Fig. 5. ZrO_2 grain diameter distribution curves for the composites with different ZrO_2 contents: (a) 10.5 vol% ZrO_2, and (b) 50 vol% ZrO_2.

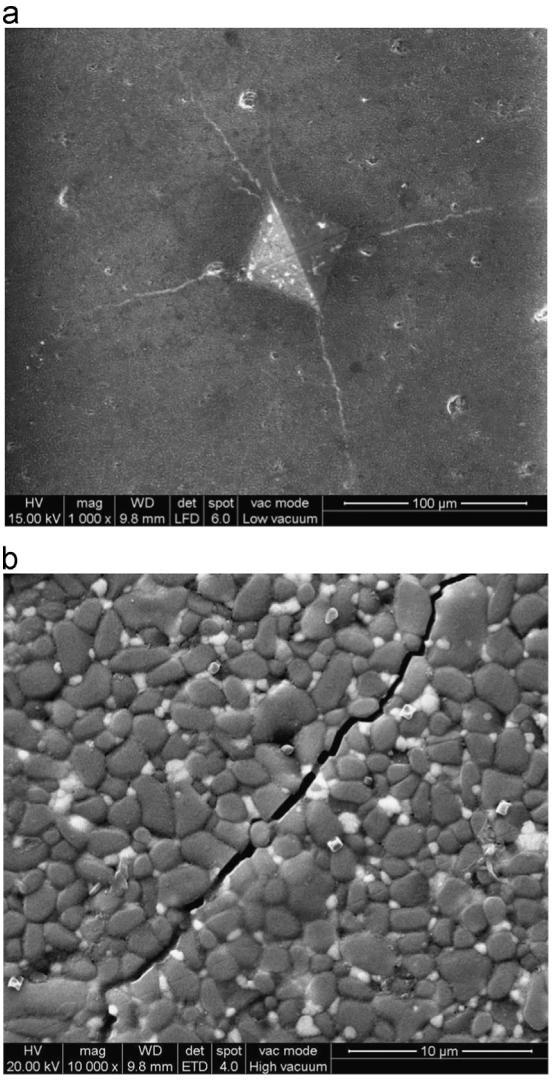

Fig. 6. (a) SEM micrograph of Vickers indentation in Al_2O_3 sintered at 1600 °C, and (b) SEM micrograph of 10.5ZN composite, showing the crack propagation path.

Table 4
Relative sintered density of the different samples at 1600 °C.

ZrO_2 content (vol%)	Al_2O_3–Y–PSZA (% TD[a])	Al_2O_3– Y–PSZ (% TD[a])	Al_2O_3–ZN (% TD[a])
0	97.36	97.36	97.36
10.5	97.79	97.65	97.70
22	98.62	98.57	
50	98.70	98.65	

[a] Theoretical density.

the intermediate sintering stage but also decreased the ZrO_2 grain growth at the final sintering stage.

Table 4 shows the sintered density of the bodies at 1600 °C for the different ZrO_2 contents. The final sintered density of pure Al_2O_3 was 97.36% TD. The substitution of Al_2O_3 either by Y–PSZA or Y–PSZ up to 22 vol% increased the relative sintered density, over 22 vol% ZrO_2 the sintered density remained nearly constant; this behavior was related with the Al_2O_3 grain growth at the final sintering stage. For Y–PSZ and Y–PSZA contents lower than 22 vol% the rapid Al_2O_3 grain growth at the final sintering stage (Table 2) reduced the sintering rate resulting in relative sintered density values close to that of Al_2O_3. Since 22 and 50 vol% ZrO_2 effectively decreased the rate of Al_2O_3 grain growth (Table 2) higher sintered densities could be achieved. Although the fine ZrO_2 grains in 10.5ZN effectively reduced the Al_2O_3 grain growth up to 1600 °C (Table 2), the relative sintered density of 10.5ZN was similar to that of 10.5Y–PSZ and 10.5Y–PSZA. This behavior could be explained taking into account the lower packing density of the 105ZN green compact (Table 1).

3.3. Mechanical properties

Fig. 6a shows a scanning electron micrograph of Vickers indentation in Al_2O_3 sintered at 1600 °C. The Al_2O_3 with its large grain size showed a crack pattern disruption and it was accordingly unsuitable for hardness and fracture toughness measurements by the indentation technique. According to Anstis et al. [10] for coarse grained materials the fracture pattern is more susceptible to disruption from local-failure events. Anisotropy in the fracture seemed to be absent in all the composites samples as cracks extended from four corners. In Fig. 6b a crack extension from the corner of an indent in a composite with 10.5 vol% ZrO_2 can be observed, it shows that the crack propagation path in the composites was intragranular.

Fig. 7 shows the Vickers hardness (Hv) versus the ZrO_2 content for the composites prepared with Y–PSZ and Y–PSZA, the Hv value of 10.5ZN was also shown. For the composites produced with Y–PSZ and Y–PSZA a maximum hardness was found at 22 vol%

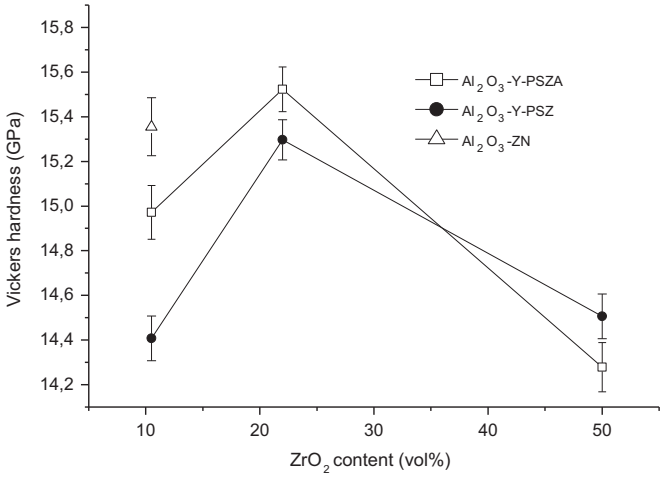

Fig. 7. Vickers hardness versus the ZrO_2 content for the different composites.

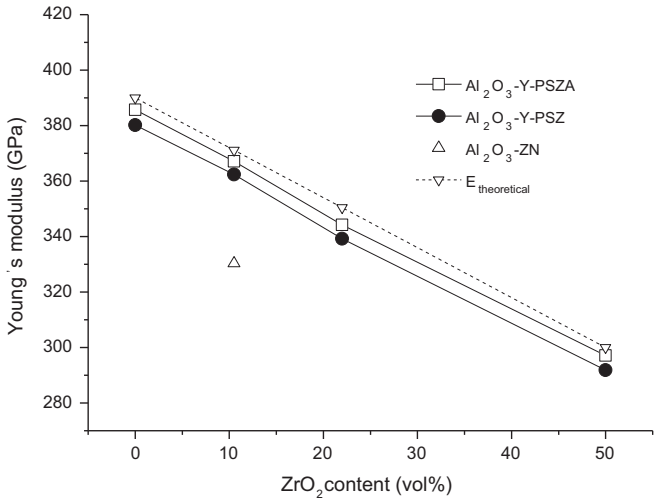

Fig. 8. Young's modulus (E) as a function of the ZrO_2 content for Al_2O_3 and the different composites. The dash line indicated the theoretical E values.

Table 5
Percentages of monoclinic ZrO_2 (m-ZrO_2) after sintering at 1600 °C at the surface and fractured surface in the different composites.

Composites	m-ZrO_2 (%) at surface	m-ZrO_2 (%) at fractured surface
10.5Y–PSZA	0.8	0.8
10.5Y–PSZ	1.2	1.2
10.5ZN	27.4	27.4
22Y–PSZA	1.1	1.1
22Y–PSZ	1.2	1.2
50Y–PSZA	1.3	9.5
50Y–PSZ	1.4	11.3

ZrO_2. For ZrO_2 content lower than 22 vol% the increase in the Al_2O_3 average grain diameter over 1 μm decreased the Hv values (Table 2 and Fig. 7). According to Rice et al. [11] the generally accepted trend was that Hv increased with decreasing the grain size (G) (e.g., $Hv \propto G^{-1/2}$) at finer G. As we have explained for the composites with 10.5 vol% ZrO_2, the Al_2O_3 grain growth became lesser as the ZrO_2 grain size decreased, consequently the lower Al_2O_3 average grain diameter of 10.5ZN compared with 10.5Y–PSZ and 10.5Y–PSZA resulted in higher Hv values (Table 2 and Fig. 7). Although the Al_2O_3 mean grain diameters of the composites with 22 and 50 vol% ZrO_2 were low, the Hv values for 50 vol% ZrO_2 were markedly lower than those of 22 vol% ZrO_2; this was due to the greater substitution of Al_2O_3 by the lower hardness ZrO_2 in the composites.

Table 5 lists the percentages of monoclinic ZrO_2 (m-ZrO_2) after sintering at 1600 °C for the different composites. X-ray analysis of all the composites containing 3 mol% Y_2O_3 stabilized ZrO_2 (Y–PSZ and Y–PSZA) revealed that the percentage of m-ZrO_2 retained at room temperature was 0.8–1.4% with the remainder (99.2–98.6%) as tetragonal ZrO_2; whereas for 10.5ZN, in which unstabilized ZrO_2 was obtained by the Zr (IV) precursor, 27.4% of the ZrO_2 was present as the monoclinic phase and 72.6% was t-ZrO_2. Analysis of Raman spectrum in sintered alumina–10 wt% zirconia (≈ 7 vol% ZrO_2) produced with unstabilized ZrO_2 [7] revealed the presence of about 25 vol% of m-ZrO_2 and 75 vol% of t-ZrO_2. Besides, Requena et al. [5] observed a high retention of t-ZrO_2 when the zirconia grain size in sintered Al_2O_3/ZrO_2 (4 vol% ZrO_2) layers was below 1 μm. A critical grain size exists, linked to the yttria concentration, above which spontaneous t–m transformation of grains takes place [2]; this critical size markedly decreased in the absence of Y_2O_3 stabilizer. Consequently, the observation that some of the t-ZrO_2 transformed to m-ZrO_2 after sintering of 10.5ZN indicated that a fraction of the unstabilized ZrO_2 grains might be above the critical size required for the transformation. In fact, we have observed (Fig. 5a) that 10.5ZN contained a low percentage of ZrO_2 grains with diameters in the range 0.75–1 μm, which could be transformed to the monoclinic phase during cooling.

Fig. 8 shows Young's modulus (E) as a function of the ZrO_2 content for Al_2O_3 and the different composites. The expected modulus were calculated by the rule of mixture, using the values of 390 GPa for Al_2O_3 and 210 GPa for t-ZrO_2 [12]; these calculated values are also included in Fig. 8. The addition of the lower elastic modulus ZrO_2 to Al_2O_3 decreased the elastic modulus of the composites. For the composites produced using 3 mol% Y_2O_3 stabilized ZrO_2 (Y–PSZ and Y–PSZA) a nearly linear decrease of E with increasing the ZrO_2 content was found; the E values were scarcely lower than those estimated by the rule of mixture due to the presence of some residual porosity. However, a comparison between the composites with 10.5 vol% ZrO_2 revealed a drastic decrease in E for the 10.5ZN composite. This indicated that the transformation from tetragonal to monoclinic phase after sintering in 10.5ZN occurred concurrently with the formation of microcracks. For a random array of microcracks with radius c, it has been shown that the young's modulus (E) is given by [13]

$$E = E_0/\left(1 + 1.8Nc^3\right) \tag{4}$$

where E_0 is Young's modulus of the uncracked material and N is the microcrack density. Therefore, E decreased with the introduction of microcracks; transmision electron microscopy of these materials shows that the monoclinic particles are also twinned [13].

Fig. 9 shows the critical fracture toughness (K_{1c}) as a function of the ZrO_2 content for the composites produced with Y–PSZ and Y–PSZA. The K_{1c} of the 10.5ZN was also included for comparison. For the composites produced with Y–PSZ and Y–PSZA a slightly increase in K_{1c} with increasing the ZrO_2 content from 10.5 to 22 vol% ZrO_2 was found followed by a significant increase with further increasing in the ZrO_2 concentration from 22 to 50 vol%. Table 5 shows the percentage of m-ZrO_2 at the surface and fractured surface in the different composites; the percentage of m-ZrO_2 increased after fracture only for the composites with 50 vol% ZrO_2. Thus, this ZrO_2 concentration promoted the t–m transformation under stress and increased K_{1c}. In fact, the alumina containing 10.5 and 22 vol% Y–PSZ and Y–PSZA exhibited K_{1c} values comparable to that of alumina ceramics (about 4 MPa $m^{1/2}$ [7]), indicating that no stress-induced transformation toughening

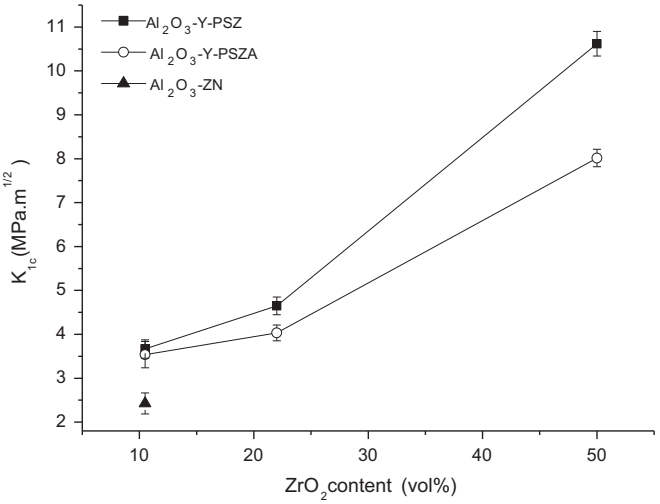

Fig. 9. Critical fracture toughness (K_{1c}) as a function of the ZrO_2 content for the different composites.

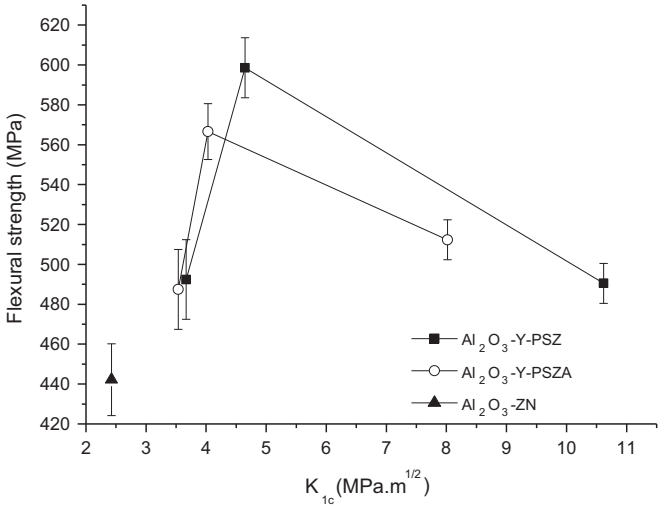

Fig. 10. Flexural strength versus the fracture toughness for the different composites.

occurred during catastrophic crack growth. The K_{1c} values of 10.5Y–PSZA and 10.5Y–PSZ were in accordance with those measured by Szutkowska [7] who obtained a similar fracture toughness value of sintered alumina–10 wt% zirconia ($\approx$ 7 vol% ZrO_2) produced with 3 mol% yttria–partially stabilized zirconia with respect to that of sintered pure alumina. On the contrary, for the composites with 50 vol% ZrO_2, K_{1c} values of 8.06 and 10.66 $MPam^{1/2}$ for 50Y–PSZA and 50Y–PSZ were obtained. This behavior was a result of crack tip shielding by the dissipation of strain energy in the transformation zone surrounding the crack.

As it was shown in Table 3*** increasing the ZrO_2 content over 22 vol% resulted in a substantial increase in the main grain diameter of ZrO_2. The tetragonal phase becomes easier to transform with increasing their size and the transformation toughening contribution increases [14]. Thus, the increase in K_{1c} with increasing the ZrO_2 content from 22 to 50 vol% was a result of the larger ZrO_2 grain size of the composites with 50 vol% ZrO_2 together with their lower elastic modulus (Table 3 and Fig. 8). The lower elastic modulus reduced the constraint of the ZrO_2 grains and allowed the transformation to proceed. For the composites with 50 vol% ZrO_2 with the lowest elastic modulus, a ZrO_2 main grain diameter of about 0.8–0.9 μm at 1600 °C promoted the stress-induced tetragonal–monoclinic transformation. The greater ZrO_2 average grain diameter of 50Y–PSZ with respect to 50Y–PSZA (Table 3) produced a greater contribution of transformation toughening leading to higher K_{1c} values.

Szutkowska [7] determined that the fracture toughness of sintered alumina–10 wt% zirconia composites obtained with unstabilized ZrO_2 exhibited a higher value with respect to that of sintered alumina–10 wt% zirconia produced with 3 mol% yttria–partially stabilized zirconia. He found intergranular crack path passing over the zirconia grains in alumina–10 wt% zirconia with unstabilized ZrO_2 as a consequence he explained that the main mechanisms for toughening in this composite were grain bridging and crack deflection. On the contrary, in the present study the K_{1c} value of the 10.5ZN composite was lower than those of 10.5Y–PSZA and 10.5Y–PSZ. As it was mentioned the low E value of the 10.5ZN composite (Fig. 8) indicated that the t–m phase transformation after sintering occurred concurrently with the formation of microcracks. Thus, residual tensile stresses and microcracks are introduced when ZrO_2 grains autotransformed during processing. First, these additional local tensile stresses and microcracks are introduced by the volume expansion and twinning associated with the autotransformation of large ZrO_2 grain-boundary grains [15]. The residual matrix stresses are also influenced by the anisotropy in the mismatch in thermal expansion coefficients of tetragonal and monoclinic ZrO_2 with those of Al_2O_3 [15]. Second, Fig. 6b shows that the crack propagation path in the 10.5ZN composites was intragranular, then the crack interacts with these existing large ZrO_2 grains and the associated tensile strains and microcracks. These two effects resulted in lower K_{1c} values of 10.5ZN compared with 10.5Y–PSZ and 10.5Y–PSZA.

Fig. 10 shows the flexural strength versus the fracture toughness for the different composites. Below 22 vol% ZrO_2 (K_{1c} less than 5 $MPam^{1/2}$) the strength decreased with decreasing the composite sintered density (Table 4), thus, the strength was limited by flaw size; whereas above 22 vol% ZrO_2 ($K_{1c} > 5$ $MPam^{1/2}$) the strength was limited by stress-actived phase transformation. This means that the stress to initiate transformation is lower than the fracture stress; therefore, transformation occurs preferentially [16]. Thus, the maximums in the curves indicated a transition from flaw-size control of strength at low toughness to transformation limited strength at higher values of toughness.

4. Conclusions

1. The increase in the Y–PSZA or Y–PSZ contents from 0 to 22 vol% markedly reduced the Al_2O_3 grain growth at the final sintering stage; as a consequence, higher sintered densities and hardness could be achieved; for 50 vol% ZrO_2 lower hardness values were obtained.
2. 2-A significant increase in K_{1c} with increasing the ZrO_2 content over 22 vol% ZrO_2 was obtained by the stress-induced phase transformation in partially stabilized ZrO_2 particles dispersed in Al_2O_3.
3. For the composites with 50 vol% ZrO_2, the 0.3 wt% Al_2O_3 content in the starting Y–PSZ powder not only increased the sintering rate at the intermediate sintering stage but also decreased the ZrO_2 grain growth at the final sintering stage.
4. The greater ZrO_2 mean grain diameter of 50Y–PSZ with respect to 50Y–PSZA produced a greater contribution of transformation toughening leading to higher K_{1c} values.
5. Below 22 vol% ZrO_2, the flaw size limited the strength; whereas, above 22 vol% ZrO_2 the strength was limited by the stress activated phase transformation.
6. For 10.5 vol% ZrO_2, the smaller ZrO_2 grains produced by using the Zr (IV) precursor were more effective in preventing the Al_2O_3 grain growth resulting in higher hardness. However, the

tetragonal–monoclinic (t–m) transformation of some unstabilized ZrO_2 grains during cooling reduced the young's modulus and fracture toughness.

References

[1] S. Olhero, I. Ganesh, P. Torres, F. Alves, J.M.F. Ferreira, J. Am. Ceram. Soc. 92 (1) (2009) 9–16.
[2] C. Piconi, G. Maccauro, Biomaterials 20 (1999) 1–25.
[3] K. Matsui, T. Yamakawa, M. Uehara, N. Enomoto, J. Hojo, J. Am. Ceram. Soc. 91 (6) (2008) 1888–1897.
[4] H.L. Calambás Pulgarin, M.P. Albano, Ceram. Int. 40 (2014) 5289–5298.
[5] J. Requena, R. Moreno, J.S. Moya, J. Am. Ceram. Soc. 72 (8) (1989) 1511–1513.
[6] H.L. Calambás Pulgarin, L.B. Garrido, M.P. Albano, Ceram. Int. 39 (6) (2013) 6657–6667.
[7] M. Szutkowska, J. Mater. Process. Technol. 153–154 (2004) 868–874.
[8] D. Balzar, N.C. Popa, Rigaku J. 22 (2005) 16–25.
[9] J. Wang, R. Raj, J. Am. Ceram. Soc. 73 (5) (1990) 1172–1175.
[10] G.R. Anstis, P. Chantikul, B.R. Lawn, D.B. Marshall, J. Am. Ceram. Soc. 64 (9) (1981) 533–538.
[11] R.W. Rice, C.C. Wu, F. Borchelt, J. Am. Ceram. Soc. 77 (10) (1994) 2539–2553.
[12] A. Rafferty, A.M. Alsebaie, A.G. Olabi, T. Prescott, J. Colloid Interface Sci. 329 (2009) 310–315.
[13] D.J. Green, J. Am. Ceram. Soc. 65 (12) (1982) 610–614.
[14] H.J. Hannink, P.M. Kelly, B.C. Muddle, J. Am. Ceram. Soc. 83 (3) (2000) 461–487.
[15] P.F. Becher, J. Am. Ceram. Soc. 66 (7) (1983) 485–488.
[16] M.V. Swain, L.R.F. Rose, J. Am. Ceram. Soc. 69 (7) (1986) 511–518.